Received: 30 June 2021 | Accepted: 11 December 2021 | Published online: 11 February 2022

DOI: 10.1002/saj2.20366

Soil Science Society of America Journal

SPECIAL SECTION: STABILITY OF MINERAL–ORGANIC MATTER ASSOCIATIONS UNDER VARYING BIOGEOCHEMICAL CONDITIONS

Localized alteration of ferrihydrite natural organic matter coprecipitates following reaction with Fe(II)

Nadia Noor | **Aaron Thompson**

Dep. of Crop and Soil Sciences, Univ. of Georgia, Athens, GA 30602, USA

Correspondence
Aaron Thompson, Dep. of Crop and Soil Sciences, Univ. of Georgia, Athens, GA 30602, USA.
Email: aaront@uga.edu

Assigned to Associate Editor Ravi Kukkadapu.

Abstract

Coprecipitation of natural organic matter (NOM) with ferrihydrite (Fh) can alter the trajectory of Fe(II)-catalyzed transformation. High C/Fe molar ratio Fh-NOM coprecipitates are expected to resist transformation completely and preserve organic matter (OM). To explore how heterogeneous NOM would influence this process, we reacted low (0.8) and high (1.8) C/Fe molar ratio Fh-NOM coprecipitates (synthesized with a ^{13}C-labeled plant litter extract) with 2 mM Fe(II) for 1 and 14 d under anoxic conditions and examined changes in the solid phase with Mössbauer spectroscopy (MBS) and secondary electron images using scanning transmission electron microscope. Mössbauer spectroscopy data suggests Fe(II) interaction with coprecipitates increases Fe mineral crystallinity, as did lower molar C/Fe ratios and longer aging times. However, de novo crystal phase development was only observed (via secondary electron images) in the Fe(II)-reacted coprecipitates and only when the organic carbon (OC) loading was low. For example, the low C/Fe coprecipitate developed localized lath-like crystal phases after 1 d of reaction with Fe(II), while the lath-like phases only developed in the high C/Fe coprecipitates after they lost some NOM (C/Fe ratio decreased from 1.8 to 0.7) and reacted with Fe(II) for 14 d. In addition, partial exchange of coprecipitate ^{13}C-NOM for C in the media (likely the organic PIPES buffer) occurred in all treatments but was accentuated by reaction with Fe(II), suggesting coprecipitate OM composition likely evolves over time, especially when exposed to Fe(II). Our findings suggest that Fe(II) mediated Fh-NOM transformation is highly dynamic and has the potential to influence the stability of NOM in Fh.

1 | INTRODUCTION

Ferrihydrite (Fh) is a common short-range-ordered (SRO) Fe(III) phase in soils and sediments (Cornell & Schwertmann, 2003; Jambor & Dutrizac, 1998). Ferrihydrite is thermodynamically unstable and will transform into more stable iron (oxyhydr)oxide minerals such as goethite, hematite, magnetite, and lepidocrocite over time (Kukkadapu et al., 2003; Schwertmann & Murad, 1983). The sorption of Fe(II)$_{(aq)}$ to Fh accelerates this transformation through a process of electron transfer and atom exchange (Boland et al., 2014; Hansel et al., 2005; Pedersen et al., 2005; Williams & Scherer, 2004). Although many studies have examined Fe(II)-catalyzed transformation of Fh, there is no consensus regarding the transformation or crystallization pathway to product minerals (Boland et al., 2014; Hansel et al., 2005), as minor

---

Abbreviations: B_{hf}, hyperfine field strength; EDS, energy-dispersive X-ray spectroscopy; Fh, ferrihydrite; MBS, Mössbauer spectroscopy; MS, magnetic susceptibility; NOM, natural organic matter; OC, organic carbon; OM, organic matter; SRO, short-range-ordered.

changes in the geochemical conditions, such as pH, $Fe(II)_{(aq)}$ concentration, the presence of cations and counterions, and organic ligands, can alter the composition of the secondary minerals (Boland et al., 2014; Chen et al., 2015; Hansel et al., 2005; Jones et al., 2009; Liu et al., 2016; ThomasArrigo et al., 2018; ThomasArrigo et al., 2019; Zhou et al., 2018).

In the natural environment, especially in biologically active soils and sediments that have dissolved organic matter (OM), Fh is typically coprecipitated with natural organic matter (NOM) (Chen et al., 2014; Lalonde et al., 2012). Association of organic carbon (OC) can decrease the available surface area of Fh and also block the adsorption of Fe(II) (Chen et al., 2014; Eusterhues et al., 2008; Jones et al., 2009), which is a major factor for the formation of secondary minerals (Boland et al., 2014). A coprecipitate C/Fe molar ratio >2.8 is likely to result in complete blockage of the adsorption sites and prevent Fe(II) adsorption in mineral surface (Chen et al., 2014), and the threshold value to prevent transformation is 1.6 (Chen et al., 2015). Despite a consensus that OM can interfere with Fe(II)-mediated Fh transformation, significant uncertainty remains regarding the specific interactions (Chen et al., 2015; ThomasArrigo et al., 2018; ThomasArrigo et al., 2019; Zhou et al., 2018). For example, some studies report coprecipitated OM retards Fh transformation progressively with increasing C/Fe molar ratios and secondary mineral formation dependent on Fe(II) concentrations (Chen et al., 2015), whereas other studies suggest longer reaction times and higher Fe(II) concentrations can cause Fh-OM transformation even when the initial C/Fe molar ratios are above 1.6 (Pedersen et al., 2005; ThomasArrigo et al., 2018). While, it is well accepted that various organic functional groups can drive transformations in consistent trajectories (Sheng et al., 2020; ThomasArrigo et al., 2019), our understanding of how Fh-OM coprecipitates behave when exposed to Fe(II) is largely based on experiments with single organic ligands or relatively homogenous OM isolates (Daugherty et al., 2017; Royer et al., 2002). It remains unclear how Fh-NOM coprecipitates with more complex OM profiles will behave. In our previous study, we found that the reaction of Fe(II) with Fh coprecipitated with Suwannee River natural organic matter (SRNOM) resulted in electron exchange between the $Fe(II)_{(aq)}$ and Fe(III) and some minor increases in the Fe phase crystallinity, increased particle size, and aggregation (Zhou et al., 2018). Another recent study showed that Fh-SRNOM coprecipitates went through an electron exchange process after reacting with Fe(II) without secondary mineral transformation but decreased their ability to retain nickel (Ni) (Zhou et al., 2021). These findings make it clear that changes are occurring in the Fh-NOM coprecipitates during reaction with Fe(II) that effect Fh behavior. There is, however, is considerable uncertainty on how those changes will manifest for more complex OM. The majority of this uncertainty arises from experiments using various types of NOM as a C source for the coprecipitates. Resolving the Fe(II)-mediated mineral transformation of Fh-NOM is critical for predicting the long-term effect of OM on the mineral binding of various constituents of interest.

Core Ideas

- Fe(II)-catalyzed transformation of ferrihydrite-natural organic matter (Fh-NOM) is governed by C/Fe molar ratios.
- Localized morphological transformations often take place in lieu of complete transformations.
- Exchange of OC from Fh-NOM and the soil solution is likely.
- Loss of NOM can reduce Fe.

To address this, we examined the effects of NOM concentration and Fe(II) exposure (aging) time on NOM and Fe composition of Fh-NOM coprecipitates. We hypothesized that the C/Fe ratio and Fe(II) exposure time will govern the transformation product composition. To test this, we synthesized Fh-NOM coprecipitates at low and high C/Fe ratios that, based on prior literature, should promote and hinder Fh transformation, respectively. Furthermore, we used ^{13}C-labled NOM {extracted from ^{13}C-labled Bermudagrass [*Cynodon dactylon* (L.) Pers.]} as the source of C in the coprecipitates to distinguish coprecipitated NOM from the organic PIPES buffer in the media. Along with the elemental analysis of the coprecipitates before and after reacting with Fe(II), we examined the solids using Mössbauer spectroscopy (MBS) and secondary electron images using an ultrahigh-resolution scanning transmission electron microscope.

2 | MATERIALS AND METHODS

2.1 | Preparation of ^{13}C labeled dissolved organic matter

Labeled dissolved organic matter was prepared by extracting ^{13}C-labeled Burmudagrass litter with water. Briefly, a pulse labeling method was used to label 'Tifton-85' bermudagrass (*C. dactylon* × *C. nlemfuencis*) with $^{13}CO_2$ (99.999 atom%, Cambridge Isotope Laboratories Inc.). Bermudagrass was grown in flats of C-free sand with some residual potting medium under greenhouse conditions for 4 wk. All flats were fertilized with 0.7 mmol $(^{15}NH_4)_2SO_4$ once a week. For ^{13}C pulse labeling, bermudagrass was transported to a Conviron growth chamber with a temperature of 35 °C and CO_2 concentration of 500 mg L^{-1} maintained using a Qubit G400-2 gas mixing system coupled with a S157 infrared

CO_2 analyzer (Kingston). Pulse labeling was carried out once a week for 6 wk. Bermudagrass was exposed to $^{13}CO_2$ for 8 h with a flow rate of $^{13}CO_2$ ~0.5 L min^{-1}. Labeled aboveground biomass was harvested and immediately frozen. The frozen material was freeze-dried and ground using Wiley mill to <1 mm. Ground materials were mixed with ultrapure 18.2 MΩ water with a solid to water ratio of 1/20 (w/v). The mixture was shaken at 140 rpm in a horizontal shaker for 48 h and filtered through a 0.45 μm polyvinylidene fluoride membrane filter. The total OC concentration and ^{13}C isotope content was measured and later diluted with ultrapure water to achieve the required concentration to prepare the coprecipitates. Molecular composition characterization of dissolved NOM was previously done using ultrahigh-resolution mass spectroscopy (Chen et al., 2020). Briefly, the NOM was comprised predominantly of aliphatic compounds (76%) and lignin-derived carboxyl-rich alicyclic molecules (23%) with mean population O/C, H/C, and DBE values of 0.44 ± 0.12, 1.60 ± 0.22, and 6.31 ± 3.04, respectively.

2.2 | Ferrihydrite and Fh-NOM coprecipitates synthesis

All the chemicals used in this study were laboratory grade. Ferrihydrite was synthesized by dissolving $Fe(NO_3)_3.9H_2O$ in ultrapure water and pH was adjusted to 7 using 1 M KOH (Schwertmann & Cornell, 2008). The Fh-NOM coprecipitates, with an initial solution C/Fe molar ratio of 0.8 or 1.8, were prepared by following the methods described by Chen et al. (2014). Briefly, the required amount of $Fe(NO_3)_3.9H_2O$ was mixed with labeled ^{13}DOC solution under vigorous stirring. The pH of the suspension was raised from ~2.0 to 7 by slowly adding 0.1 M KOH. Synthesized Fh and Fh-NOM coprecipitate were centrifuged at 12,000 × *g* for 10 min and washed twice using degassed ultrapure water and stored in the glove box (97% N_2 and 3% H_2) for at least 48 h to remove O_2 gas before reacting with Fe(II) in our experiments as described below.

2.3 | Reacting Fh-NOM coprecipitates with Fe(II)

Freshly synthesized, moist Fh and Fh-NOM coprecipitate were resuspended in anoxic PIPES (1,4-piperazinediethane sulfonic acid) buffer (10 mM, pH 7) and stirred for 1 d inside the glovebox (filled with 97% N_2 and 3% H_2) to remove residual O_2. A portion of the Fh and Fh-NOM coprecipitates were reacted with Fe(II) in 100-ml opaque serum bottles containing 33.6 mg of total Fe (as an Fh-NOM slurry) and 60 ml of anoxic PIPES buffer (10 mM, pH 7). $FeSO_4.7\,H_2O$ was added to the bottle (except the controls) to obtain a final Fe(II) concentration of 2 mM (Chen et al., 2015). The reaction was carried out in the anoxic glove box on a rotatory shaker in two batches: one reacted with Fe(II) for 24 h (henceforth 'fresh') and one reacted for 14 d (henceforth 'aged'). After the reactions, the Fe(II)-reacted Fh and Fh-NOM samples were rinsed with degassed 18.2 MΩ ultrapure water twice by centrifuging them at 10,000 × *g* for 10 min. After washing the samples, a small amount of degassed water was added to maintain a moist slurry and the samples were stored at −20 ˚C before analysis.

2.4 | Analysis for ^{13}C, total C, and Fe in the solid

The total C and ^{13}C isotope content of the solid phase were measured by lyophilizing a portion of the solid sample, crimped in a tin capsule, and analyzing it in a Thermo Flash 2000 elemental analyzer coupled to a Thermo Delta V isotope ratio mass spectrometer via Thermo Conflo IV open split interface. The total Fe content was measured using inductively coupled plasma mass spectrometry (Perkin Elmer, Elan 9000) after the dissolution of 2 mg coprecipitates in 5 ml 30% HCl for 1 h and volume up to 30 ml with 1% HCl (Chen et al., 2014). We calculated the amount of ^{13}C-NOM in the solid samples (P ^{13}C-NOM in solid) using a two-source mixing model.

$$P\ ^{13}C_{NOM}\ \text{in solid} = \frac{x\left[^{13}C\right]\ Fh_{NOM} - x\left[^{13}C\right]\ Fh}{x\left[^{13}C\right]\ NOM - x\left[^{13}C\right]\ Fh} \times 100$$

Where, $x[^{13}C]Fh_{NOM}$ and $x[^{13}C]Fh$ are atom fractions of ^{13}C isotope in the coprecipitates and ^{13}C content of the Fh, respectively; $x[^{13}C]NOM$ is the initial atom fraction of ^{13}C content of the bermudagrass extract.

2.5 | Mössbauer analysis

Mössbauer spectroscopy analysis was done using a 50-mCi ^{57}Co/Rh source under 5, 13, and 35 K to characterize Fe in the coprecipitates after reacting with Fe(II) along with the unreacted controls. Collected solid samples were washed twice with ultrapure water by placing the samples in a falcon centrifuge tube with a sufficient amount of water following gentle shaking and centrifuged at 3,000 × *g* for 10 min. The supernatant was then poured off, the samples were placed in an O-ring, sealed between two pieces of Kapton tape, and immediately frozen in a −20 ˚C freezer. The MBS results were analyzed using Recoil software (http://recoil.sourceforge.net), and spectra fitting was done using Voigt-based fitting. In addition, mass-specific magnetic susceptibility (MS) measurement was collected on coprecipitates at 295 K in a

TABLE 1 Molar C/Fe ratio of the synthesized coprecipitates (initial) and after reacting with Fe(II) and aging (final) in PIPES buffer. Fraction of ^{13}C natural organic matter (NOM) represents percentage ^{13}C NOM remaining in the coprecipitates after reaction with Fe(II) and aging

Treatment		Initial C/Fe ratio	Fraction of ^{13}C NOM (final)	Final C/Fe ratio
		mol/mol	%	mol/mol
Fresh	Ferrihydrite (Fh)	–	n.d.	0.4
	Fh with Fe(II)	–	n.d.	0.08
	Low C/Fe	0.8	88	0.9
	Low C/Fe with Fe(II)	0.8	64	1.0
	High C/Fe	1.8	81	1.8
	High C/Fe with Fe(II)	1.8	76	1.7
Aged	Fh	–	n.d.	0.5
	Fh with Fe(II)	–	n.d.	0.09
	Low C/Fe	0.8	56	0.5
	Low C/Fe with Fe(II)	0.8	34	0.5
	High C/Fe	1.8	72	0.7
	High C/Fe with Fe(II)	1.8	60	0.7

Note. n.d., not detectable.

Bartington MS meter (MS2B). Measurements were calibrated against a well-characterized standard set used previously (Thompson et al., 2011). More detailed information is provided in the Supplemental Materials.

2.6 | Secondary electron imaging

To assess the qualitative morphological variation of the Fe(II)-reacted coprecipitates vs. the unreacted control, secondary electron image analysis along with energy-dispersive X-ray spectroscopy (EDS) mapping of the coprecipitates was conducted. Images were obtained using the secondary electron detector of a scanning transmission electron microscope (STEM-Hitachi SU 9000EA) while operating with an accelerating voltage of 30 kV. The solid sample slurry was placed on a silica chip and dried overnight, which was later analyzed under the microscope. A secondary electron detector was used for collecting the images and EDS spectra were recorded with Oxford Ultim Extreme software.

3 | RESULTS

3.1 | Total Fe and C content of the coprecipitates

Total Fe, C, and ^{13}C isotope (i.e., coprecipitated C) contents were measured in the solids before and after reaction with Fe(II) (Table 1; Supplemental Table S1). In the fresh samples, all treatments and unreacted controls retained nearly their initial measured C/Fe ratios of either 0.8 or 1.8 for the low and high treatments, respectively. However, in the aged samples, the C/Fe molar ratios decreased. For the aged–low coprecipitates, the C/Fe molar ratio decreased from 0.8 to 0.5, and for the aged–high coprecipitates it decreased from 1.8 to 0.7. Interestingly, reaction with Fe(II) drove up the total C content of the fresh and aged–low coprecipitates relative to the unreacted controls, although the Fe(II)-reacted coprecipitates lost more ^{13}C NOM at the expense of unlabeled OC from the media than their paired unreacted controls. For instance, the OC in the Fe(II)-reacted fresh–low coprecipitate was comprised of 64% NOM, whereas the unreacted pared control was comprised of 88% NOM. For the aged coprecipitates, which also experienced a decrease in C/Fe ratio, the loss of NOM fraction was even greater, with the aged–low coprecipitates comprising 34% NOM after reaction with Fe(II) vs. 56% NOM in its unreacted control. The high C/Fe treatments had similar trends, although the relative fractions of NOM after reaction were greater (Table 1). Finally, our pure Fh controls gained some OC after 1 and 14 d of aging and the values were higher than the Fe(II)-reacted Fh. The PIPES buffer could be the source of C although we did not see any change in the pH content of the reactors. This increased C content did not appear to influence the transformation of Fh, as the sample completely transformed to lath-like crystals after 14 d (Supplemental Figure S1). This measured OC in the Fh treatment may also have been an experimental or analytical contaminant.

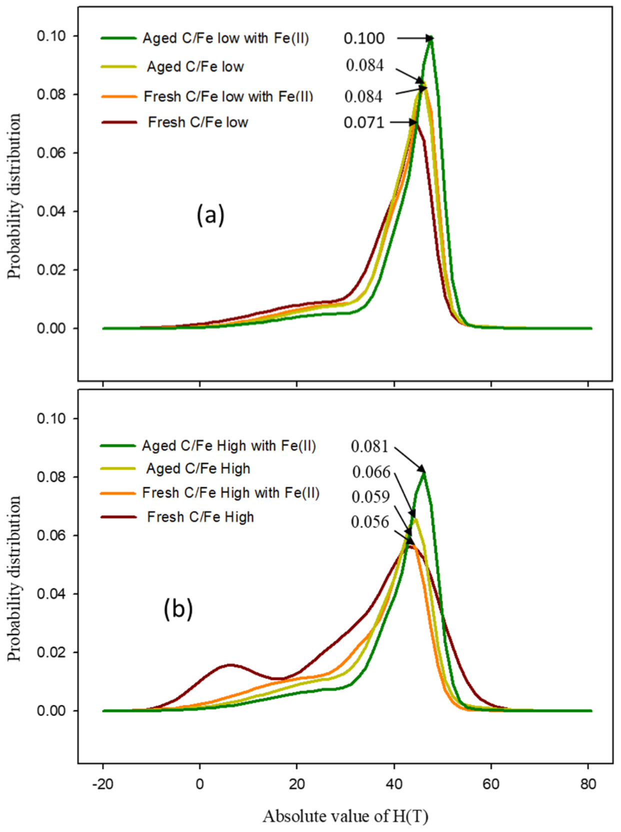

FIGURE 1 Probability density distribution of the hyperfine field of the (a) low C/Fe [Fe(II)-reacted and unreacted] and (b) high C/Fe [Fe(II)-reacted and unreacted] coprecipitates collected at 13 K temperature using Mössbauer spectroscopy. The *y*-axis values of the peak are indicated with the arrows

3.2 | Changes in Fh-NOM crystallinity and morphology

3.2.1 | Mössbauer spectroscopy

Mössbauer spectra collected at 35, 13, and 5 K were used to characterize changes in the crystallinity of the Fe(II)-reacted coprecipitates relative to the unreacted controls (Figure 1; Supplemental Figures S2–S6; Supplemental Tables S2–S10). At the lowest collection temperature (5 K), the Fe(III) populations of all the samples were magnetically ordered into a sextet (Supplemental Figures S2–S6). Portions of the sample forming a sextet at higher temperatures (13 and 35 K) are more crystalline than the remaining portions that require lower temperatures to magnetically order and this can be used to compare the relative crystallinity of the Fh-NOM coprecipitates (Thompson et al., 2006, 2011).

At 5 K, the MBS parameters of the Fh control sample are characteristic of 2-line Fh (chemical shift of 0.47 mm s^{-1}; quadrupole splitting of −0.01 mm s^{-1}; hyperfine field strength (B_{hf}) of 48.1 T; Supplemental Table S2) (Kukkadapu et al., 2003). In the coprecipitate samples, as expected (Chen et al., 2015), the inclusion of NOM lowers a 5 K sextet's average B_{hf} to between 46.2 and 47.7 T across all samples, with samples reacted with Fe(II) having B_{hf} values ∼0.78 T higher than their unreacted controls (Supplemental Tables S1–S10). At 5 K, we also see two other consistent trends: (a) all of the low C/Fe ratios samples have higher B_{hf} values (by 0.65–1.36 T) than their respective high C/Fe samples, and (b) the aged samples have higher B_{hf} values than their respective fresh samples (by 0.53–1.3 T) (Table 2; Supplemental Tables S2–S10). Higher B_{hf} values are consistent with higher crystallinities (Murad & Cashion, 2011) in the Fe(II)-reacted samples, in samples with low C/Fe ratios, and those aged for longer periods. These higher crystallinities could derive from a variety of reasons (i.e., less substitution, stronger interparticle interactions, greater particle size, etc.) (Eusterhues et al., 2008).

A separate measure of sample crystallinity is the temperature dependence of the sextet formation (i.e., blocking temperature), with more crystalline samples ordering into a full sextet at higher temperatures than lower crystallinity samples (Murad & Cashion, 2011). Using this metric, we find similar results to those obtained by examining the B_{hf} values. Based on blocking temperature, the most crystalline coprecipitate sample is the aged–low coprecipitate reacted with Fe(II), which has a sextet (OxHy) already beginning to form at 35 K (Figure 1; Supplemental Figure S4) (note, for comparison, that it is even more crystalline than our Fh control, which at 35 K the MBS is modeled with only a collapsed sextet). The least crystalline sample, based on ordering temperature, would be the fresh–high-unreacted coprecipitate, which requires ∼10% of the spectral area as a doublet to get a good fit at 13 K (Figure 1; Supplemental Figure S5). Already, sextet ordering temperature matches the trends in sextet hyperfine field strength at the extremes of our coprecipitate samples, with aging, low C/Fe ratio, and reaction with Fe(II) conferring greater crystallinity. To evaluate the remaining samples, we examine the sextets at 13 K, where they display a range of ordering conditions, with the more crystalline samples exhibiting sextets that resemble those at 5 K and the less-crystalline samples exhibiting large partially collapsed sextet features (highly broadened features that extend across the velocity range). We modeled these 13 K sextets with three components and then evaluated the distribution of these components across the sextet (Figure 1). In these graphs, higher probability values (*y* axis) for the peak of the sextet indicate a sharper sextet with less spectral area in the collapsed portion [i.e., what would be a (b)OxHy component], whereas values along the *x* axis are the B_{hf} values of the distribution. We also expect more crystalline phases to have higher peak positions on the *x* axis, but we have already evaluated the B_{hf} of the phases more precisely at 5 K. Here instead, we focus on the *y* axis height of the main peak. In this case, we see, similar to the evaluation of crystallinity at 5 K using the B_{hf} values, that the fraction of sextet area in the peak B_{hf} value is higher in all cases for Fe(II)-reacted samples

TABLE 2 Selected Mössbauer sextet parameters of unreacted and Fe(II)-reacted C/Fe coprecipitates and Ferrihydrite (Fh) control along with the morphological changes observed in secondary electron image analysis

Sample	Treatment	Avg. B_{hf} 5 K[a]	Peak B_{hf} 5 K[b]	Percentage of 13 K sextet at peak B_{HF}[c]	Electron microscope–observed morphological change
		———T———		%	
Fresh–low	Unreacted	46.4	48.1 ± 0.6	7.1	–
	Fe(II)-reacted	47.1	48.7 ± 0.9	8.3	Lath-like localized phases
Fresh–high	Unreacted	45.0	46.6 ± 0.3	5.6	–
	Fe(II)-reacted	45.7	47.4 ± 0.6	5.9	Crystallinity increased
Aged–low	Unreacted	46.9	48.6 ± 0.3	8.3	–
	Fe(II)-reacted	47.7	49.5 ± 0.2	10.0	Fe spherules development
Aged–high	Unreacted	46.2	47.6 ± 0.2	6.6	–
	Fe(II)-reacted	47.0	48.8 ± 0.2	8.2	Lath-like localized phases
Fh (control)	Unreacted	48.1	49.5 ± 0.3	11.6	Lath phase formation

Note. A detailed description is present in Supplemental Tables S2–S10.

[a] Average magnitude of the hyperfine field strength (B_{hf}) in Torr (T).

[b] Peak value of the magnitude of the hyperfine field distribution in Torr (T).

[c] Percentage of the total hyperfine field distribution of the sextet at 13 K present in at the peak.

(compared with their unreacted controls), higher in all cases for the low C/Fe samples relative to the corresponding high C/Fe samples, and higher in the aged samples relative to the corresponding fresh samples (Figure 1, Table 2).

3.2.2 | Secondary electron imaging

Secondary electron images of the Fe(II)-reacted coprecipitates indicate variations in the morphology and crystallinity of the coprecipitates (Figures 2 and 3; Supplemental Figures S7–S12). The morphological appearance of all the coprecipitates after reacting with Fe(II) changed compared with the paired unreacted controls. Similarly, there were morphological differences that suggest changes in phase crystallinity between low and high C/Fe ratios and between samples aged for different time periods in presence of Fe(II). In our control Fh, the mineral started to transform after reacting with Fe(II) for 1 d and after 14 d, completely transformed into lath-like structure resembling lepidocrocite structures (Jelle et al., 2016) (Supplemental Figure S1). Unlike the Fh mineral, transformations in the coprecipitate were limited to localized development of new morphologies, and in no case did those changes extend over full coprecipitate structure. The largest differences in the amount of crystallite development occurred between the low C/Fe and high C/Fe samples (Figures 2 and 3). After reacting with Fe(II) for 1 d, the bulk structure of the low C/Fe coprecipitates remained similar to the unreacted samples, but localized nanosized crystals formed as aggregates with a lath morphology suggestive of lepidocrocite or goethite (Figure 2) (Jelle et al., 2016; Schwertmann & Thalmann, 1976). In some places, the bulk aggregates were laminated in lath-like crystals (Figure 2b), while in other places nano-lath-like phases (<10 nm) developed (Figure 2c), and elsewhere, there appeared 10–65-nm-sized, lath-like crystals (Figure 2d) similar to lepidocrocite structures reported by ThomasArrigo et al. (2019). Upon aging for 14 d with Fe(II), these lath-like crystal phases disappeared in the low C/Fe coprecipitates (Supplemental Figure S7). In their place, spherical nanosized phases appeared on the bulk structure along with 80- to 100-nm-sized mineral clusters in some parts of the samples. Above 8 nm, Fh is thermodynamically unstable at room temperature and transforms into nanogoethite or hematite (Hiemstra, 2015; Navrotsky et al., 2008), which suggests these mineral clusters could be nanogoethite (Jelle et al., 2016). Given prior reports of magnetite phases forming during Fe(II) reaction with Fh (Hansel et al., 2005), we assessed the possibility of magnetite formation by measuring the MS (Supplemental Table S11). The MS values of the coprecipitate ranged from 1.7×10^{-7} to 20.4×10^{-7} m^3 kg^{-1} except for the fresh Fe(II)-reacted Fh, which had a higher MS value (5.6×10^{-5} m^3 kg^{-1}). Typically, Fh, goethite, and hematite have MS values ~5.0×10^{-7} m^3 kg^{-1}. The usual MS values for magnetite or maghemite are ~4.5×10^{-4} m^3 kg^{-1} (Michel et al., 2010; Thompson et al., 2011), suggesting magnetite or maghemite did not form in the coprecipitates.

The high C/Fe coprecipitates have quite a different trajectory of crystallite formation. After 1 d of reaction with Fe(II), the high C/Fe coprecipitates largely retained their unreacted bulk morphologies, with the exception of the formation of some minor iron spherules (1.5 μm) (Franke et al., 2009) (Supplemental Figure S8). However, after 14 d of reaction with Fe(II), the coprecipitates began to resemble the low C/Fe coprecipitates with the formation of <10 nm-sized, lath-like crystals (Figure 3) (Jelle et al., 2016).

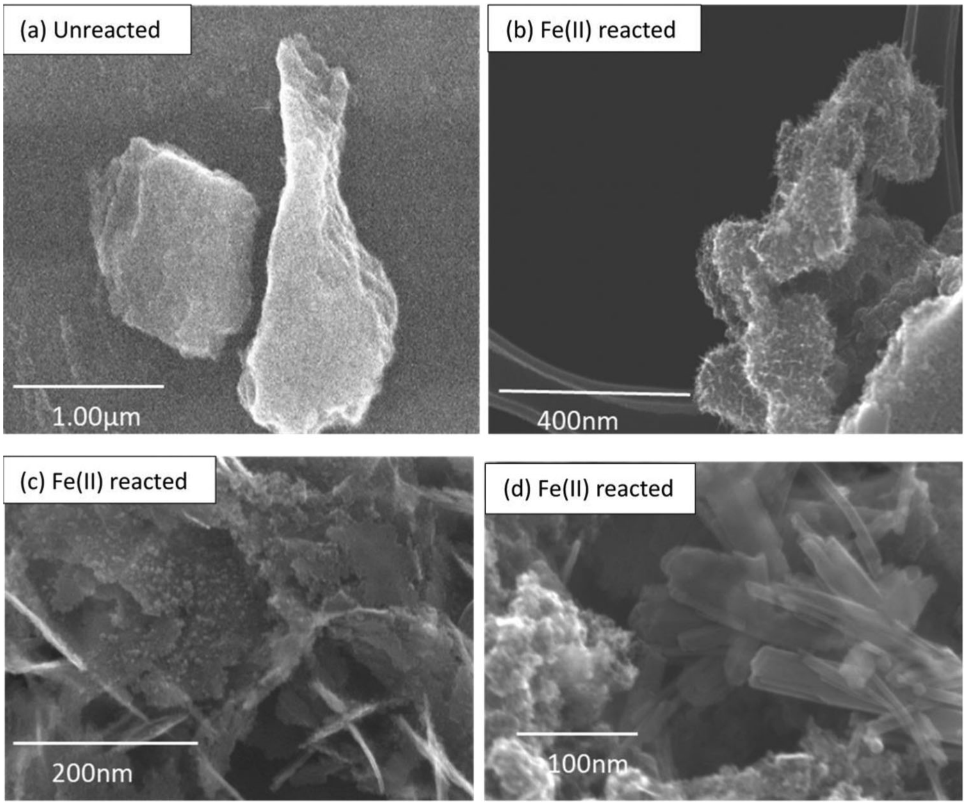

FIGURE 2 Secondary electron images of the fresh–low C/Fe (a) unreacted and (b–d) Fe(II)-reacted coprecipitates showing lath-like phase development in the coprecipitates

4 | DISCUSSION

4.1 | Carbon dynamics during Fe(II) reaction with coprecipitates

Our experiment involved the incubation of Fh-NOM coprecipitates generated using ^{13}C-labeled NOM in a solution containing an unlabeled organic PIPES (1,4-Piperazinediethanesufonic acid) buffer with natural C isotopic composition. We found that the coprecipitates released OC between the 1 and 14 d incubation time, and this release was substantial for the high OC-loaded coprecipitates. While the low C/Fe molar ratio coprecipitates decreased from 0.8 to 0.5, the high C/Fe molar ratio decreased from 1.8 to 0.7 during the aging process. Along with this OC release, we also observed an exchange of OC between the coprecipitates (^{13}C-labeled) and the PIPES buffer solution in the reactor vials and this exchange was higher for the Fe(II)-reacted coprecipitates (Supplemental Table S1).

The protection of OC by minerals is contingent on several factors including inherent chemical recalcitrance of the OM, the degree of inclusion of the OM into secondary aggregate structures, the distribution of OM on the mineral surface that influences the amount of direct contact and intimate association with the mineral surfaces, and the amount of mineral specific surface area available for the OM (Baldock & Skjemstad, 2000; Eusterhues et al., 2003). Changes in any of these factors can result in the release of OC from the mineral structure.

Fe(II) reaction with the high-OC-containing coprecipitate can also result in a slight decrease in the C/Fe ratio (Chen et al., 2015; ThomasArrigo et al., 2019). ThomasArrigo et al. (2017) has found that the coprecipitate C/Fe ratio decreased (from 1.2 to 0.9) after extended (70 d) reaction with 1 mM Fe(II), and similar to our study, they observed the development of lath-like phases in the coprecipitates. In our study, because OC was released from both the unreacted and reacted coprecipitates, it was not driven by the reaction with Fe(II) and not likely related to the increase in crystallinity of the Fe(II)-reacted coprecipitates during aging. The higher release of OC during the aging can also result from the structural flaw of the coprecipitates, but in our preliminary study we kept high C/Fe coprecipitates aging in water for over 3 mo without a decrease in the C/Fe ratio (data not shown). Therefore, we believe that the OC release in our study resulted from the interaction between the PIPES buffer and the coprecipitated OC. Although we do not have information regarding the molecular composition of the solution in the reactors after the experiment, we do know that OC exchange occurred between

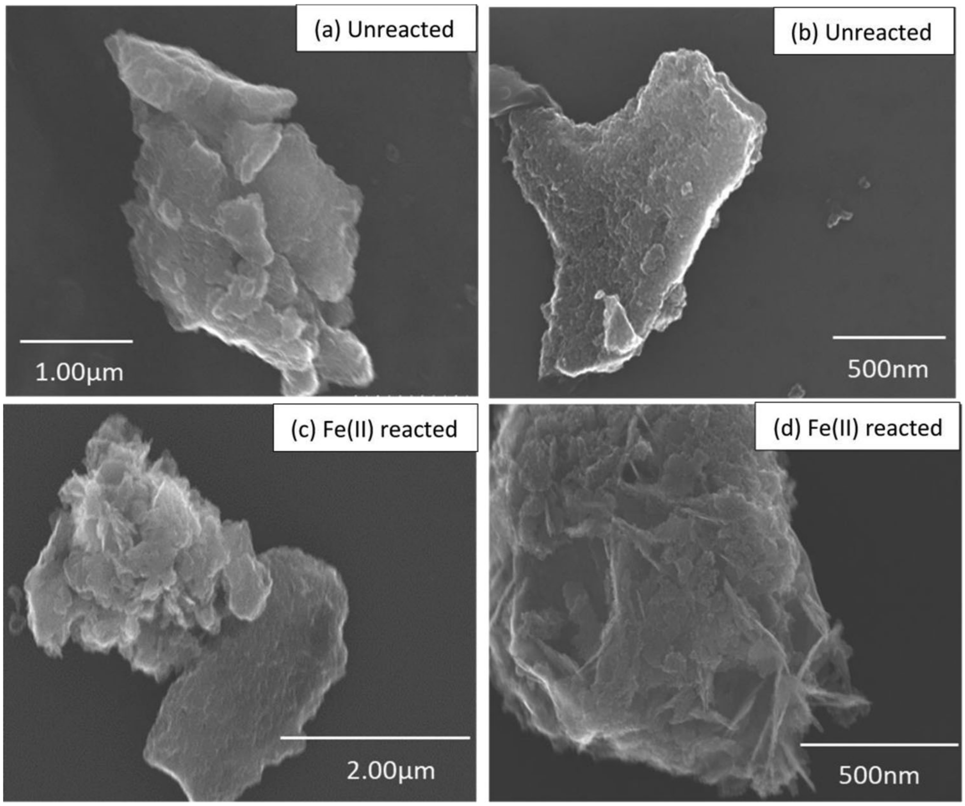

FIGURE 3 Secondary electron images of aged–high C/Fe (a,b) unreacted and (c,d) Fe(II)-reacted coprecipitates showing localized crystal structure development with lath-like phases in the coprecipitates

the coprecipitates and the PIPES buffer, and perhaps this drove the change in coprecipitate-associated OC over the 14 d of reaction.

Prior work has suggested PIPES buffer does not react significantly with Fe phases (Henneberry et al., 2012). However, our Fh-NOM coprecipitates progressed through a sequence whereby they first accumulated PIPES from the solution (after 1 d of reaction) with concomitant loss of NOM and then lost a large fraction of both the PIPES and initial C sources as the reactions proceeded to 14 d (Table 1). Reaction with Fe(II) uniformly drove the greater loss of the NOM but in some cases higher accumulation of PIPES. The point of zero charge of Fh is between 7 and 9 pH (Cornell & Schwertmann, 2003; Parks, 1965). In our reactor vials, the pH was set at 6.9 ± 0.1, which likely resulted in a slight positive surface charge on the Fh; however, the NOM contains negatively charged carboxyl groups (pKa 3–4) and thus the point of zero charge of the coprecipitates was likely between 4 and 7 (ThomasArrigo et al., 2019), and the surface was likely negatively charged. The pKa value for the PIPES buffer is 6.7 at 25 ˚C, which gives it a buffering range of 6.1–7.5. Therefore, the charged surface could result in the formation of a surface complex with the buffer. Chen et al. (2015) observed no change in the total C content of Fh-NOM coprecipitates after reacting them with Fe(II) in a PIPES buffer but later found that the resulting transformation products desorbed significant C when exposed to an anoxic 0.1 M NaH_2PO_4 desorption solution. An exchange between coprecipitate OM and PIPES could have occurred in the Chen et al. (2015) study and not been detected as they did not use isotopes to distinguish C sources.

4.2 | Localized mineral transformation

The presence of Fe(II) increased the crystallinity of the Fh-NOM coprecipitates, enhancing the effect of lower molar C/Fe ratios and longer aging times had on increasing crystallinity (Figures 2 and 3; Table 2). These higher crystallinities in samples with lower C/Fe ratios, longer aging times, or reaction with Fe(II) are clearly evident in the MBS spectra (by two separate measures) (Figure 1; Table 1). In the secondary electron images, only samples reacted with Fe(II) exhibited visual development of new crystallites, where some treatments developed localized lath-like crystal phases (Figures 2 and 3) and others only showed relatively higher aggregated structure formation (Supplemental Figures S7–S8) than the unreacted controls. These observed variations in the Fe(II)-reacted coprecipitates also reflect the combined effect of C/Fe ratio and aging time.

By definition, more coprecipitation of OM in Fe minerals should lower the MBS-derived assessment of crystallinity as the excess OM must disrupt the development of long-range crystal structure (Eusterhues et al., 2008; Schwertmann, 1966). This is also true for the incorporation of Al, Si, or other foreign ions in Fe minerals and is covered well in prior literature (Doelsch et al., 2000; Hansel et al., 2011; Jones et al., 2009; Mayer & Jarrell, 1996; Schwertmann, 1970). Similarly, longer aging times of SRO mineral phases (such as Fh) will usually generate increases in crystallinity (Johnston & Lewis, 1983). In our study here, our interest lies primarily with the reaction with Fe(II) and its intersection with the C/Fe ratio and the aging process. Because we only see the development of lath-like crystals following Fe(II) reaction in the low-OM-containing coprecipitates but see changes in the MBS spectra consistent with increasing crystallinity, even in the unreacted aged samples, we surmise that Fe(II)-promoted crystallinity changes are more surface oriented in low-OM-containing coprecipitates than Ostwald-ripening via sample aging (Hiemstra, 2018; Hiemstra et al., 2019).

Prior work has clearly illustrated that coprecipitates with lower C/Fe ratios will undergo transformation to more crystalline phases after reaction with Fe(II) (Chen et al., 2015; Eusterhues et al., 2014; Jones et al., 2009; ThomasArrigo et al., 2018). Generally, C/Fe ratios below ∼1 allow crystallinity increases following reaction with Fe(II) (Chen & Sparks, 2018; ThomasArrigo et al., 2017; Zhou et al., 2018), although a precise cutoff can be elusive and likely based on OM (and Fe mineral) type. Higher OM loading on Fh is thought to hinder Fe(II) sorption to the Fh surface by blocking the mineral surface sites or micropore entrances and thus prevent Fh transformation (Chen et al., 2014; Chen et al., 2015; Eusterhues et al., 2014; Hiemstra et al., 2019). Higher OM loading has also been shown to alter rates of biotic Fh reduction (Shimizu et al., 2013) in some cases, decreasing rates by inhibiting the direct contact of the microbes to the Fh surface (Eusterhues et al., 2014) or increasing rates if OM can be used as an electron shuttle (Cooper et al., 2017). Under abiotic conditions, Chen et al. (2015) showed Fe(II) induced no secondary mineral transformation in Fh coprecipitates formed with OM extracted from highly weathered soils (C/Fe ratio of 1.6), whereas, ThomasArrigo et al. (2017) suggested C/Fe ratios near 2.5 were required to prevent mineral transformation when the Fh coprecipitated with polygalacturonic acid or OM from freshwater flocs. In our study, coprecipitates with a C/Fe ratio of 1.8 did not exhibit crystallite development (in the secondary electron images) after reacting with Fe(II) for 1 d, whereas those with a C/Fe ratio of 0.8 did form new crystals. However, after reaction for 14 d, initial C/Fe of 1.8 containing coprecipitates developed lath-like crystal structures, but these coprecipitates also experienced a decrease in their C/Fe ratio from the loss of OC (Table 1; Supplemental Table S1) (decrease of C/Fe ratio of 1.8–0.7). This decrease in the C/Fe ratio likely allowed Fe(II) to adsorb on the Fh surface and promote localized mineral transformations. The EDS mapping data (Supplemental Figure S10) also illustrates that the de novo lath-like phases formed on the coprecipitates were relatively C poor. This observation that the aged–high C/Fe coprecipitates and the fresh–low C/Fe coprecipitates behaved similarly suggests that at some point during the 14-d reaction time, the high C/Fe coprecipitates lost sufficient C to allow Fe(II)-catalyzed transformations to begin in localized regions.

5 | CONCLUSION

We have found that the reaction of Fe(II) can drive crystallinity changes in Fh-NOM coprecipitates, with lower C/Fe ratios and longer aging times enhancing this effect. Further, we see that Fe(II)-induced de novo crystal formations occurred only in localized regions of the coprecipitates and that lower C/Fe ratios were a prerequisite for their formation. This was especially evident in our high C/Fe sample, which resisted de novo crystal formation at 1 d of reaction with Fe(II) but then developed lath-like crystals after 14 d of reaction in conjunction with a loss of OM and decrease in C/Fe ratio. Our study also illustrates that OC exchange can occur between the coprecipitated C and the other C sources in solution. Such OC exchange is likely a very common phenomenon in the natural environment and likely affects the composition of OM associated with SRO minerals such as Fh. The interplay between minerals and organic matter is likely much more dynamic than typically appreciated and the potential for changes in soil solution conditions (i.e., redox shifts, changes in dissolved organic matter composition or concentrations) are likely to have implications for the stability of mineral associated organic matter, especially for redox-active SRO Fe phases.

ACKNOWLEDGMENTS

The authors are grateful to the National Science Foundation for financial support of the research (EAR-1331846, EAR-1331841, DEB-1457761, and EAR-1451508). We thank Dr. Eric Formo and the Georgia electron microscopy lab for assistance in the Secondary electron image analysis. We thank Dr. Michelle M. Scherer for reviewing the early version of the manuscript. We also thank three anonymous reviewers and associate editor Dr. Ravi Kukkadapu for helpful comments that substantially improved the manuscript.

AUTHOR CONTRIBUTIONS

Nadia Noor: conceptualization; data curation; formal analysis; investigation; methodology; writing – original draft; writing – review & editing. Aaron Thompson: conceptualization; formal analysis; funding acquisition; investigation; methodology; project administration; resources; supervision; writing – original draft; writing – review & editing.

CONFLICT OF INTEREST

The authors declare no conflicts of interest.

ORCID

Nadia Noor https://orcid.org/0000-0002-5464-5635
Aaron Thompson https://orcid.org/0000-0001-6301-7377

REFERENCES

Baldock, J., & Skjemstad, J. (2000). Role of the soil matrix and minerals in protecting natural organic materials against biological attack. *Organic Geochemistry*, *31*, 697–710. https://doi.org/10.1016/S0146-6380(00)00049-8

Boland, D. D., Collins, R. N., Miller, C. J., Glover, C. J., & Waite, T. D. (2014). Effect of solution and solid-phase conditions on the Fe(II)-accelerated transformation of ferrihydrite to lepidocrocite and goethite. *Environmental science & technology*, *48*, 5477–5485. https://doi.org/10.1021/es4043275

Chen, C., Dynes, J. J., Wang, J., & Sparks, D. L. (2014). Properties of Fe-organic matter associations via coprecipitation versus adsorption. *Environmental Science & Technology*, *48*, 13751–13759. https://doi.org/10.1021/es503669u

Chen, C., Hall, S. J., Coward, E., & Thompson, A. (2020). Iron-mediated organic matter decomposition in humid soils can counteract protection. *Nature Communications*, *11*, 2255. https://doi.org/10.1038/s41467-020-16071-5

Chen, C., Kukkadapu, R., & Sparks, D. L. (2015). Influence of coprecipitated organic matter on $Fe^{2+}{}_{(aq)}$–catalyzed transformation of ferrihydrite: Implications for carbon dynamics. *Environmental Science & Technology*, *49*, 10927–10936. https://doi.org/10.1021/acs.est.5b02448

Chen, C., & Sparks, D. L. (2018). Fe(II)-induced mineral transformation of ferrihydrite–organic matter adsorption and coprecipitation complexes in the absence and presence of As(III). *ACS Earth and Space Chemistry*, *2*, 1095–1101. https://doi.org/10.1021/acsearthspacechem.8b00041

Cooper, R. E., Eusterhues, K., Wegner, C.-E., Totsche, K. U., & Küsel, K. (2017). Ferrihydrite-associated organic matter (OM) stimulates reduction by Shewanella oneidensis MR-1 and a complex microbial consortia. *Biogeosciences*, *14*, 5171–5188. https://doi.org/10.5194/bg-14-5171-2017

Cornell, R. M., & Schwertmann, U. (2003). *The iron oxides: Structure, properties, reactions, occurrences and uses*. John Wiley & Sons.

Daugherty, E. E., Gilbert, B., Nico, P. S., & Borch, T. (2017). Complexation and redox buffering of iron(II) by dissolved organic matter. *Environmental Science & Technology*, *51*, 11096–11104.

Doelsch, E., Rose, J., Masion, A., Bottero, J. Y., Nahon, D., & Bertsch, P. M. (2000). Speciation and crystal chemistry of iron(III) chloride hydrolyzed in the presence of SiO_4 ligands. 1. An Fe K-edge EXAFS study. *Langmuir*, *16*, 4726–4731. https://doi.org/10.1021/la991378h

Eusterhues, K., Hädrich, A., Neidhardt, J., Küsel, K., Keller, T., Jandt, K., & Totsche, K. (2014). Reduction of ferrihydrite with adsorbed and coprecipitated organic matter: Microbial reduction by Geobacter bremensis vs. abiotic reduction by Na-dithionite. *Biogeosciences*, *11*, 4953–4966. https://doi.org/10.5194/bg-11-4953-2014

Eusterhues, K., Rumpel, C., Kleber, M., & Kögel-Knabner, I. (2003). Stabilisation of soil organic matter by interactions with minerals as revealed by mineral dissolution and oxidative degradation. *Organic Geochemistry*, *34*, 1591–1600. https://doi.org/10.1016/j.orggeochem.2003.08.007

Eusterhues, K., Wagner, F. E., Häusler, W., Hanzlik, M., Knicker, H., Totsche, K. U., Kögel-Knabner, I., & Schwertmann, U. (2008). Characterization of ferrihydrite-soil organic matter coprecipitates by X-ray diffraction and Mossbauer spectroscopy. *Environmental Science & Technology*, *42*, 7891–7897. https://doi.org/10.1021/es800881w

Franke, C., Kissel, C., Robin, E., Bonté, P., & Lagroix, F. (2009). Magnetic particle characterization in the Seine river system: Implications for the determination of natural versus anthropogenic input. *Geochemistry, Geophysics, Geosystems*, *10*. https://doi.org/10.1029/2009GC002544

Hansel, C. M., Benner, S. G., & Fendorf, S. (2005). Competing Fe(II)-induced mineralization pathways of ferrihydrite. *Environmental Science & Technology*, *39*, 7147–7153. https://doi.org/10.1021/es050666z

Hansel, C., Learman, D., Lentini, C., & Ekstrom, E. (2011). Effect of adsorbed and substituted Al on Fe(II)-induced mineralization pathways of ferrihydrite. *Geochimica et Cosmochimica Acta*, *75*, 4653–4666. https://doi.org/10.1016/j.gca.2011.05.033

Henneberry, Y. K., Kraus, T. E., Nico, P. S., & Horwath, W. R. (2012). Structural stability of coprecipitated natural organic matter and ferric iron under reducing conditions. *Organic Geochemistry*, *48*, 81–89. https://doi.org/10.1016/j.orggeochem.2012.04.005

Hiemstra, T. (2015). Formation, stability, and solubility of metal oxide nanoparticles: Surface entropy, enthalpy, and free energy of ferrihydrite. *Geochimica et Cosmochimica Acta*, *158*, 179–198. https://doi.org/10.1016/j.gca.2015.02.032

Hiemstra, T. (2018). Surface structure controlling nanoparticle behavior: Magnetism of ferrihydrite, magnetite, and maghemite. *Environmental Science: Nano*, *5*, 752–764.

Hiemstra, T., Mendez, J. C., & Li, J. (2019). Evolution of the reactive surface area of ferrihydrite: Time, pH, and temperature dependency of growth by Ostwald ripening. *Environmental Science: Nano*, *6*, 820–833.

Jambor, J. L., & Dutrizac, J. E. (1998). Occurrence and constitution of natural and synthetic ferrihydrite, a widespread iron oxyhydroxide. *Chemical Reviews*, *98*, 2549–2586. https://doi.org/10.1021/cr970105t

Jelle, A. A., Hmadeh, M., O'Brien, P. G., Perovic, D. D., & Ozin, G. A. (2016). Photocatalytic properties of all four polymorphs of nanostructured iron oxyhydroxides. *ChemNanoMat*, *2*, 1047–1054. https://doi.org/10.1002/cnma.201600251

Johnston, J., & Lewis, D. (1983). A detailed study of the transformation of ferrihydrite to hematite in an aqueous medium at 92°C. *Geochimica et Cosmochimica Acta*, *47*, 1823–1831. https://doi.org/10.1016/0016-7037(83)90200-4

Jones, A. M., Collins, R. N., Rose, J., & Waite, T. D. (2009). The effect of silica and natural organic matter on the Fe(II)-catalysed transformation and reactivity of Fe(III) minerals. *Geochimica et Cosmochimica Acta*, *73*, 4409–4422. https://doi.org/10.1016/j.gca.2009.04.025

Kukkadapu, R. K., Zachara, J. M., Fredrickson, J. K., Smith, S. C., Dohnalkova, A. C., & Russell, C. K. (2003). Transformation of 2-line ferrihydrite to 6-line ferrihydrite under oxic and anoxic conditions. *American Mineralogist*, *88*, 1903–1914. https://doi.org/10.2138/am-2003-11-1233

Lalonde, K., Mucci, A., Ouellet, A., & Gélinas, Y. (2012). Preservation of organic matter in sediments promoted by iron. *Nature*, *483*, 198–200. https://doi.org/10.1038/nature10855

Liu, C., Zhu, Z., Li, F., Liu, T., Liao, C., Lee, J.-J., Shih, K., Tao, L., & Wu, Y. (2016). Fe(II)-induced phase transformation of ferrihydrite: The inhibition effects and stabilization of divalent metal cations. *Chemical Geology*, *444*, 110–119. https://doi.org/10.1016/j.chemgeo.2016.10.002

Mayer, T. D., & Jarrell, W. M. (1996). Formation and stability of iron(II) oxidation products under natural concentrations of dissolved silica. *Water Research*, *30*, 1208–1214. https://doi.org/10.1016/0043-1354(95)00265-0

Michel, F. M., Barrón, V., Torrent, J., Morales, M. P., Serna, C. J., Boily, J.-F., Liu, Q., Ambrosini, A., Cismasu, A. C., & Brown, G. E. (2010). Ordered ferrimagnetic form of ferrihydrite reveals links among structure, composition, and magnetism. *Proceedings of the National Academy of Sciences*, *107*, 2787–2792. https://doi.org/10.1073/pnas.0910170107

Murad, E., & Cashion, J. (2011). *Mössbauer spectroscopy of environmental materials and their industrial utilization*. Springer Science & Business Media.

Navrotsky, A., Mazeina, L., & Majzlan, J. (2008). Size-driven structural and thermodynamic complexity in iron oxides. *Science*, *319*, 1635–1638. https://doi.org/10.1126/science.1148614

Parks, G. A. (1965). The isoelectric points of solid oxides, solid hydroxides, and aqueous hydroxo complex systems. *Chemical Reviews*, *65*, 177–198. https://doi.org/10.1021/cr60234a002

Pedersen, H. D., Postma, D., Jakobsen, R., & Larsen, O. (2005). Fast transformation of iron oxyhydroxides by the catalytic action of aqueous Fe(II). *Geochimica et Cosmochimica Acta*, *69*, 3967–3977. https://doi.org/10.1016/j.gca.2005.03.016

Royer, R. A., Burgos, W. D., Fisher, A. S., Unz, R. F., & Dempsey, B. A. (2002). Enhancement of biological reduction of hematite by electron shuttling and Fe(II) complexation. *Environmental Science & Technology*, *36*, 1939–1946. https://doi.org/10.1021/es011139s

Schwertmann, U. (1966). Inhibitory effect of soil organic matter on the crystallization of amorphous ferric hydroxide. *Nature*, *212*, 645–646. https://doi.org/10.1038/212645b0

Schwertmann, U. (1970). The influence of simple organic anions on the formation of goethite and haematite from amorphous ferric hydroxide. *Geoderma*, *3*, 207–214. https://doi.org/10.1016/0016-7061(70)90020-0

Schwertmann, U., & Cornell, R. M. (2008). *Iron oxides in the laboratory: Preparation and characterization*. John Wiley & Sons.

Schwertmann, U., & Murad, E. (1983). Effect of pH on the formation of goethite and hematite from ferrihydrite. *Clays and Clay Minerals*, *31*, 277–284. https://doi.org/10.1346/CCMN.1983.0310405

Schwertmann, U., & Thalmann, H. (1976). The influence of [Fe(II)], [Si], and pH on the formation of lepidocrocite and ferrihydrite during oxidation of aqueous $FeCl_2$ solutions. *Clay Minerals*, *11*, 189–200. https://doi.org/10.1180/claymin.1976.011.3.02

Sheng, A., Liu, J., Li, X., Qafoku, O., Collins, R. N., Jones, A. M., Pearce, C. I., Wang, C., Ni, J., & Lu, A. (2020). Labile Fe(III) from sorbed Fe(II) oxidation is the key intermediate in Fe(II)-catalyzed ferrihydrite transformation. *Geochimica et Cosmochimica Acta*, *272*, 105–120. https://doi.org/10.1016/j.gca.2019.12.028

Shimizu, M., Zhou, J., Schröder, C., Obst, M., Kappler, A., & Borch, T. (2013). Dissimilatory reduction and transformation of ferrihydrite-humic acid coprecipitates. *Environmental Science & Technology*, *47*, 13375–13384. https://doi.org/10.1021/es402812j

ThomasArrigo, L. K., Byrne, J. M., Kappler, A., & Kretzschmar, R. (2018). Impact of organic matter on iron(II)-catalyzed mineral transformations in ferrihydrite–organic matter coprecipitates. *Environmental Science & Technology*, *52*, 12316–12326. https://doi.org/10.1021/acs.est.8b03206

ThomasArrigo, L. K., Kaegi, R., & Kretzschmar, R. (2019). Ferrihydrite growth and transformation in the presence of ferrous iron and model organic ligands. *Environmental Science & Technology*, *53*, 13636–13647. https://doi.org/10.1021/acs.est.9b03952

ThomasArrigo, L. K., Mikutta, C., Byrne, J., Kappler, A., & Kretzschmar, R. (2017). Iron(II)-catalyzed iron atom exchange and mineralogical changes in iron-rich organic freshwater flocs: An iron isotope tracer study. *Environmental Science & Technology*, *51*, 6897–6907. https://doi.org/10.1021/acs.est.7b01495

Thompson, A., Chadwick, O. A., Rancourt, D. G., & Chorover, J. (2006). Iron-oxide crystallinity increases during soil redox oscillations. *Geochimica et Cosmochimica Acta*, *70*, 1710–1727. https://doi.org/10.1016/j.gca.2005.12.005

Thompson, A., Rancourt, D. G., Chadwick, O. A., & Chorover, J. (2011). Iron solid-phase differentiation along a redox gradient in basaltic soils. *Geochimica et Cosmochimica Acta*, *75*, 119–133. https://doi.org/10.1016/j.gca.2010.10.005

Williams, A. G., & Scherer, M. M. (2004). Spectroscopic evidence for Fe(II)−Fe(III) electron transfer at the iron oxide−water interface. *Environmental Science & Technology*, *38*, 4782–4790. https://doi.org/10.1021/es049373g

Zhou, Z., Latta, D. E., Noor, N., Thompson, A., Borch, T., & Scherer, M. M. (2018). Fe(II)-catalyzed transformation of organic matter–ferrihydrite coprecipitates: A closer look using Fe isotopes. *Environmental Science & Technology*, *52*, 11142–11150. https://doi.org/10.1021/acs.est.8b03407

Zhou, Z., Latta, D. E., & Scherer, M. M. (2021). Natural organic matter inhibits Ni stabilization during Fe(II)-catalyzed ferrihydrite transformation. *Science of the Total Environment*, *755*, 142612. https://doi.org/10.1016/j.scitotenv.2020.142612

SUPPORTING INFORMATION

Additional supporting information may be found in the online version of the article at the publisher's website.

How to cite this article: Noor, N., & Thompson, A. (2022). Localized alteration of ferrihydrite natural organic matter coprecipitates following reaction with Fe(II). *Soil Science Society of America Journal*, *86*, 253–263. https://doi.org/10.1002/saj2.20366